THE ASTRONOMICAL JOURNAL, 122:1954–1964, 2001 October

HYDROXYL 1.563 MICRON ABSORPTION FROM STARSPOTS ON ACTIVE STARS

DOUGLAS O'NEAL[1]
Natural Sciences and Mathematics, West Liberty State College, West Liberty, WV 26074; onealdb@wlsc.edu
JAMES E. NEFF[1]
Department of Physics and Astronomy, College of Charleston, 66 George Street, Charleston, SC 29424; neffj@cofc.edu
STEVEN H. SAAR[1]
Harvard-Smithsonian Center for Astrophysics, 60 Garden Street, Cambridge, MA 02138; saar@head-cfa.harvard.edu
AND
JONATHAN K. MINES[1,2]
Department of Physics, Washington and Jefferson College, Washington, PA 15301; jkm27@pitt.edu
Received 2001 April 3; accepted 2001 June 28

ABSTRACT

We present results from a study of starspots on active stars using a pair of vibrational-rotational absorption lines of the OH molecule near 1.563 μm. We detect excess OH absorption due to dark, cool starspots on several active stars of the RS CVn and BY Dra classes. Our results for the single-lined spectroscopic binaries II Pegasi, V1762 Cygni, and λ Andromedae augment those from a previous study that used a less sensitive detector. In this study, we were able for the first time to use molecular absorption features to measure starspot properties on double-lined spectroscopic binaries. Measuring the equivalent widths of these OH lines in inactive giant and dwarf stars of spectral types G, K, and M, we find that the total equivalent width of the line pair increases approximately linearly as effective temperature decreases from 5000 to 3000 K. We measure starspot filling factors by fitting the spectra of active stars with linear combinations of comparison star spectra representing the spot and nonspot regions of the star.

Key words: stars: activity — stars: atmospheres — stars: spots — techniques: spectroscopic

1. INTRODUCTION

In previous papers (Neff, O'Neal, & Saar 1995, hereafter Paper I; O'Neal, Saar, & Neff 1996, hereafter Paper II) we develop a spectroscopic technique to measure the temperatures and total area (filling factor) of starspots on magnetically active stars. We use spectra of inactive M stars to model the spotted regions of the active star photospheres and spectra of inactive G and K stars to model the nonspotted regions. We then combine these spectra to fit the absorption bands of the TiO molecule at 7055 and 8860 Å observed from active stars.

The TiO bands, while they can be used to constrain starspot area and temperature independently, are primarily useful for spot temperatures $T_S \lesssim 4000$ K. Thus, to extend the temperature range over which starspots can be analyzed spectroscopically, we searched for temperature-dependent features diagnostic of higher temperatures. Also, in the visible, starspots are much fainter than the nonspotted photosphere of active stars, thus they only weakly affect the overall spectrum of the star. For this reason, we searched for spectral features in the near-infrared, where the spots become brighter relative to the unspotted photosphere.

After considering using the first-overtone bands of CO near 2.2 μm and various atomic lines (O'Neal & Neff 1997, hereafter ON), we chose to observe the 6397 cm^{-1} 3–1 P2e and P2f ($J = 5.5$) transitions of the OH molecule. These lines are very sensitive to temperature (Grevesse, Sauval, & van Dishoeck 1984); they are quite strong in sunspots and in the spectrum of Arcturus (Hinkle, Wallace, & Livingston 1995), but they are invisible in the solar photosphere (Wallace & Livingston 1992). There are no skyglow or atmospheric absorption lines at this wavelength (Hinkle et al. 1995). It is also an advantage to observe in the infrared because of the greater relative brightness of starspots compared with the star's photosphere; in a star with $T_S = 3500$ K and nonspot temperature $T_Q = 5000$ K, the ratio of continuum surface flux between the spot and photosphere, R_λ, is 0.11 at 7050 Å (based on models by Kurucz 1992) and 0.21 at 8850 Å, but it is 0.49 at 1.56 μm.

ON show that the combined equivalent width of this line pair increases almost linearly with decreasing temperature in both giant and dwarf stars for $T_{\rm eff}$ from 5000 to 3000 K. This makes it an ideal diagnostic for starspot properties when observed in the spectrum of a magnetically active star. ON observed a spectral region centered on this line pair using the NICMASS infrared camera at the Coudé Feed Telescope of Kitt Peak National Observatory (KPNO) In addition to inactive comparison stars, we observed three magnetically active stars of the RS CVn class (active binary systems in which at least one component is evolved): II Pegasi, λ Andromedae, and V1762 Cygni. We measured starspot filling factors similar to those found using TiO bands: 0.35–0.48 (multiple observations taken over most of one complete rotation of the star) for II Peg, 0.22–0.26 for λ And, and 0.27–0.32 for V1762 Cyg. The NICMASS observations were limited to short exposure times (12 minutes or less) to prevent saturating the detector with background emission. Because of this, signal-to-noise (S/N) values for the NICMASS spectra of II Peg were limited to ~ 50.

[1] Visiting Astronomer, Kitt Peak National Observatory, National Optical Astronomy Observatory, operated by AURA, Inc., under cooperative agreement with the National Science Foundation.
[2] Current address: Department of Physics and Astronomy, University of Pittsburgh, Pittsburgh, PA 15260.

In 1998 November–December we thus undertook more sensitive and complete observations of these OH lines. The observations presented in this paper have a wider bandpass (78 Å) than those in ON (45 Å). This bandpass allowed us to observe, in addition to the OH lines, the highly magnetically sensitive ($g = 3$) Fe I line at 1.5648 μm (a subject of future analysis). Our new observations were not as severely limited by short exposure times. In this paper, we describe observations of nine magnetically active stars, including six not studied by ON (see Table 1). For the first time using our spectral synthesis technique, we measure starspot properties on the active components of binary systems that are strongly double-lined (UX Ari, OU Gem, and HR 1099). This was aided by the relative simplicity of the OH absorption lines compared with the great complexity of the TiO absorption bands we observed previously.

2. OBSERVATIONS AND ANALYSIS

The data were obtained from 1998 November 26 to 1998 December 2 with the 2.1 m telescope at KPNO, using the Phoenix IR spectrograph (Hinkle et al. 1998). Of our eight-night observing run, five nights were clear enough to permit observations. Phoenix is a cryogenic, high-resolution IR (1 to 5 μm) spectrograph. It uses an Aladdin 512 × 1024 InSb detector array and a 63°.4, 33 line mm^{-1} echelle grating. We used an order-sorting filter of central wavelength 1.558 μm and a bandpass of approximately 0.01 μm (78.4 Å) centered on the 6397 cm^{-1} (1.563 μm) lines of the OH molecule. The dispersion of the spectra is 0.0766 Å per pixel. We achieved a resolution of ~2.5 pixels, or $R = \lambda/\Delta\lambda \approx 60{,}000$.

A tungsten source usually used for wavelength calibration yielded no emission lines in our bandpass. Wavelengths were therefore calibrated by taking a spectrum of Arcturus and using the λ scales in the Arcturus Atlas (Hinkle et al. 1995) and the National Solar Observatory solar spectral atlas (Wallace & Livingston 1991). In practice, an extremely accurate wavelength scale was not necessary for our program; all spectra were co-aligned with our Arcturus spectrum.

Bias removal and background subtraction were accomplished by taking at least two consecutive spectra of each target star with the same exposure time but illuminating different, well-separated rows of the detector. Subtracting these exposures yielded two background-free spectra of the star.

Flat-field division and extraction of the spectra were accomplished using Interactive Data Language routines (IDL) written by J. A. Valenti (2000, private communication). Averaging spectra taken consecutively (usually two for inactive comparison stars, three or more for the usually fainter active stars) resulted in S/N values of 150–180 in the continuum for our spectra.

Given wavelengths fell at different pixels on the detector on different nights of observation. After our initial data reduction, we found (primarily by comparing spectra of the same star taken on different nights) that certain pixel ranges on the detector had slightly reduced sensitivity. To address this problem, we divided each spectrum by a boxcar-smoothed (to eliminate high-frequency noise) spectrum of Rigel obtained the same night. Rigel, a hot star, has no strong absorption lines in our wavelength interval. Using this procedure led to much better fits (with the method described below) to the active star spectra. No spectrum of Rigel was obtained on December 2; we divided these spectra by the December 1 Rigel spectrum, but their normalization, and thus fits to these active star spectra, should be considered highly uncertain.

In Table 1 we list the properties of the nine active target stars. Except where noted, T_Q and T_S (the effective temperatures of the unspotted photosphere and the spots, respectively) are based on measurements reported in Paper II, and the sources for the ephemerides are given in the foot-

TABLE 1

PROPERTIES OF ACTIVE STARS

Object	HD	Sp. Type	$v \sin i$ (km s^{-1})	P_{rot} (days)	HJD ($\Phi = 0$)	T_Q (K)	T_S (K)
Evolved stars:							
V1762 Cyg.....	179094	K1 III–IV	15	28.5895[a]	2,442,479.214[a]	4550	3450
λ And	222107	G8 III–IV	6.5	53.95[b]	2,443,829.2[b]	4750	3650
II Peg	224085	K2–3 IV	23	6.72422[c]	2,443,033.47[c]	4800	3500
σ Gem	62044	K1 III	25	19.60447[d]	2,447,227.08[d]	4500	3850
UX Ari.....	21242	K0 IV/G5 V	37/6	6.43791[e]	2,440,133.766[e]	5000[e]/5500[f]	3500[e]
HR 1099	22468	K1 IV/G5 IV	40/13	2.83774 [g]	2,442,766.08[g]	4700[h]/5500[f]	3500[h]
Dwarf stars:							
Gl 171.2A.....	283750	K4 V	7.5	1.7955[i]	[i]	4500[j]	3175[j]
LQ Hya.....	82558	K2 V	21	1.601136[k]	2,448,270.0[k]	5175[j]	3650[j]
OU Gem	45088	K3 V/K5 V	5.6/5.6	6.991848[l]	2,443,846.2[l]	4925/4550[f]	?

[a] Strassmeier, Hall, & Henry 1994.
[b] Boyd et al. 1983.
[c] Vogt 1981.
[d] Bopp & Dempsey 1989.
[e] Elias et al. 1995.
[f] This paper, estimated from spectral types.
[g] Fekel 1983.
[h] Hatzes et al. 1996.
[i] Olah & Pettersen 1991; no zero HJD given.
[j] Saar et al. 2000.
[k] Jetsu 1993.
[l] Bopp et al. 1981.

TABLE 2

LOG OF OBSERVATIONS OF ACTIVE STARS AND RESULTS

Star and UT	JD (−2,400,000+)	Phase (Mid)	f_S
V1762 Cyg:			
1998 Nov 26	51,143.58	0.06	0.17 ± 0.03
1998 Nov 27	51,144.64	0.10	0.20 ± 0.05
1998 Dec 1	51,148.62	0.24	0.13 ± 0.03
λ And:			
1998 Nov 26	51,143.65	0.58	0.17 ± 0.03
1998 Nov 27	51,144.66	0.60	0.17 ± 0.03
1998 Dec 1	51,148.66	0.67	0.21 ± 0.03
II Peg:			
1998 Nov 26	51,143.69	0.12	0.37 ± 0.07
1998 Nov 27	51,144.60	0.26	0.43 ± 0.07
1998 Nov 27	51,144.79	0.28	0.45 ± 0.05
1998 Nov 30	51,147.73	0.72	0.49 ± 0.08
1998 Dec 1	51,148.58	0.85	0.38 ± 0.06
1998 Dec 1	51,148.77	0.88	0.35 ± 0.07
σ Gem:			
1998 Nov 26	51,143.93	0.79	≤0.08
1998 Nov 27	51,144.95	0.85	0.23 ± 0.04
1998 Nov 30	51,147.95	0.00	0.10 ± 0.04
1998 Dec 1	51,148.96	0.05	≤0.09
1998 Dec 2	51,149.95	0.10	0.09 ± 0.05
UX Ari:			
1998 Nov 26	51,143.83	0.19	0.26 ± 0.04
1998 Nov v27.....	51,144.71	0.33	0.11 ± 0.04
1998 Nov 30	51,147.78	0.81	0.34 ± 0.04
1998 Dec 1	51,148.68	0.95	0.42 ± 0.06
1998 Dec 2	51,149.87	0.13	0.48 ± 0.09
HR 1099:			
1998 Nov 26	51,143.86	0.27	0.07 ± 0.05
1998 Nov 27	51,144.75	0.58	0.40 ± 0.05
1998 Nov 30	51,147.82	0.67	0.11 ± 0.06
1998 Dec 1	51,148.73	0.99	≤0.05
Gl 171.2A:			
1998 Nov 27	51,144.88	[a]	0.45 ± 0.06
LQ Hya:			
1998 Nov 26	51,144.01	0.98	0.26 ± 0.04
1998 Nov 30	51,148.00	0.48	0.45 ± 0.03
1998 Dec 1	51,148.98	0.09	0.28 ± 0.07
OU Gem:			
1998 Nov 26	51,143.91	0.74	0.20 ± 0.03
1998 Nov 27	51,144.92	0.89	0.35 ± 0.05
1998 Nov 30	51,147.93	0.32	0.22 ± 0.04
1998 Dec 1	51,148.91	0.46	≤0.04

[a] No recent ephemeris available.

notes. In the case of double-lined binaries, we list properties of the more active star first; these T_S values refer to measurements by previous investigators of the active component of the binary. Table 2 is a log of our observations of these nine active stars. Each observation consists of three to six consecutive exposures, subtracted in pairs to remove background and averaged. The quantity f_S is our measured spot filling factor, the fractional spot coverage weighted by projection and limb-darkening effects. Times for each individual exposure ranged from 120 s (λ And) to 1200 s (e.g., II Peg and HD 82558).

We also observed a set of inactive comparison stars covering the range of T_Q and T_S expected for the active stars (Table 3). Photometry for the stars comes from Stauffer & Hartmann (1986) and the Bright Star Catalog (Hoffleit & Jaschek 1982). Where no H-band photometry was available, we estimated H from the spectral type and the $V-H$ colors of standard stars listed by Wamstecker (1981) and of other comparison stars with measured H magnitudes. $T_{\rm eff}$ values were computed using the methods described in Paper II and were rounded to the nearest 25 K.

In Figure 1 we present spectra of a sample of our giant and subgiant comparison stars, set on the wavelength scale of the Arcturus Atlas, with the 1.563 μm OH lines identified with an arrow. Other lines are identified in Hinkle et al. (1995). One can immediately see the increase in the strengths of the OH lines with decreasing $T_{\rm eff}$. We measured the combined equivalent width of the two OH lines for each comparison star (Fig. 2).

Figure 3 presents spectra of some of the dwarf comparison stars we observed. For the M dwarfs, we note that the OH lines are substantially weaker than in giant stars of the same temperature. The same behavior was observed for the absorption bands of TiO (Paper I).

3. RESULTS

Since OH absorption is seen in stars as warm as 5000 K and several of our active target stars have T_Q cooler than this, both the nonspot and spotted regions of the photospheres of these stars contribute to the total OH absorption strength. In addition, for any star with $v \sin i \gtrsim 15$ km s^{-1}, the OH lines are blended with nearby weak lines. (Starspots on stars with $v \sin i \approx 50$ km s^{-1} would be difficult to observe with this technique, since the OH lines would then begin to blend with the strong neighboring Fe I lines.) Nonetheless, excess absorption in the OH lines due to starspots is readily apparent in all our active star spectra. In Figure 4 we have plotted all our spectra of II Peg along with the artificially rotationally broadened spectrum of γ^2 Del, an inactive star with $T_{\rm eff}$ close to the T_Q of II Peg.

To quantify this excess OH absorption, we fit the spectra of the active stars using the STARMOD spectral synthesis code. STARMOD, written (Barden 1985) and later modified (by D. P. Huenemoerder and A. D. Welty) at Penn State, fits an observed spectrum with a linear combination of up to three model spectra. It has been used extensively (e.g., Welty & Wade 1995) to determine radial and rotational velocities and spectral types of systems of interest and to find the relative brightnesses of stars in systems of two or three components. Given a target star spectrum to fit, STARMOD constructs a model by shifting the standard-star spectra in radial velocity and by applying a standard rotational broadening function (e.g., Gray 1988) with a limb-darkening coefficient $\epsilon = 0.3$ (appropriate for the H band; Claret, Diaz-Cordoves, & Giminez 1995). The user inputs initial estimates for the radial velocity, $v_{\rm rad}$, $v \sin i$, and relative weight of each standard spectrum, which are iterated in succession until the best fit is achieved. For our purposes, $v \sin i$ was fixed to the best literature value, and the only meaning of the $v_{\rm rad}$ iteration was as a correction for slight errors that may have occurred in the alignment with the Arcturus Atlas λ scale. For SB2 systems, the $v_{\rm rad}$ of the secondary was fitted, with an initial guess based on the expected $v_{\rm rad}$ separation of the binary at the phase of the observation. In all cases but Gl 171.2A, we restricted each fit to the wavelength region $1.5615\ \mu{\rm m} \leq \lambda \leq 1.5640\ \mu{\rm m}$.

The best-fit relative weights of the two standard-star spectra computed by STARMOD are directly related to the starspot filling factor on the active star. The normalized

TABLE 3

PROPERTIES OF COMPARISON STARS

HD	HR	Name	Sp. Type	V	H	$R-I$	$T_{\rm eff}$
Giant comparison stars:							
196755.....	7896	κ Del	G2 IV	5.0	3.4	...	5550
198149.....	7957	η Cep	K0 IV	3.4	1.0[a]	0.49	4925
194013.....	7794	...	G8 III–IV	5.3	3.3	0.50	4850
19787.....	951	δ Ari	K2 III	4.4	1.7[a]	0.51	4750
197964.....	7948	γ^2 Del	K1 IV	3.9	1.5[a]	0.48	4700
197912.....	7942	52 Cyg	G9.5 III	4.2	2.2[a]	0.53	4675
8512	402	θ Cet	K0 III	3.6	1.2[a]	0.56	4650
95345.....	4291	58 Leo	K1 III	4.8	2.3	0.56	4600
73471.....	3418	σ Hya	K1 III	4.4	1.9[a]	0.56	4600
66216.....	3149	χ Gem	K2 III	4.9	2.2[a]	0.60[a]	4525
124897.....	5340	α Boo	K1.5 III	0.0	−2.8	0.65	4350
60522.....	2905	υ Gem	M0 III	4.1	0.9[a]	0.96	3925
204724.....	8225	2 Peg	M1 III	4.6	1.0[a]	1.09	3800
183630.....	7414	36 Aql	M1 III	5.0	1.4	1.09[a]	3700
44478.....	2286	μ Gem	M3 III	2.9	−1.6	1.38	3625
20720.....	1003	τ^4 Eri	M3.5 III	3.7	−1.1[a]	1.46	3600
2411	103	TV Psc	M3 III	5.1	0.4[a]	1.52	3575
123657.....	5299	BY Boo	M4.5 III	5.3	−0.1	1.66	3550
175865.....	7157	R Lyr	M5 III	4.0	−0.5	1.91	3425
94705.....	4267	VY Leo	M5.5 III	5.8	−0.4	2.09	3325
18191.....	867	RZ Ari	M6 III	5.9	−0.7	2.17	3200
Dwarf comparison star:							
20630.....	996	κ Cet	G5 V	4.8	3.3[a]	0.36	5600
101501.....	4496	61 UMa	G8 V	5.3	3.6	0.36	5550
16160.....	753	Gl 105A	K3 V	5.8	3.5	0.53	4775
28343.....	...	Gl 169	K7 V	8.3	5.8[a]	0.62	3750
79210.....	...	Gl 338A	M0 V	7.6	4.3	0.68	3675
.....	...	Gl 96	M1.5 V	9.4	5.7	0.78	3525
42581.....	...	Gl 229A	M1	8.1	4.4	0.82	3450
1326	...	Gl 15A	M2 V	8.1	4.2[a]	0.88	3375
	...	Gl 273	M4 V	9.9	5.1	1.21	3175

[a] No H-band photometry available; estimated from $T_{\rm eff}$ and V.

spectrum of the active star, $F_{\rm total}$, can be written

$$F_{\rm total} = \frac{f_S R_\lambda F_S + (1 - f_S) F_Q}{f_S R_\lambda + (1 - f_S)}, \quad (1)$$

where f_S is the spot filling factor, the total fractional projected area of spots on the observed hemisphere weighted by limb darkening, R_λ is the continuum surface flux ratio between the spot and nonspot photosphere, and F_S and F_Q are the normalized spot and nonspot comparison spectra, respectively. STARMOD calculates the best relative weights, W_S and W_Q, of the two comparison spectra, such that $F_{\rm total} = W_S F_S + W_Q F_Q$. Therefore,

$$W_Q = \frac{1 - f_S}{f_S R_\lambda + (1 - f_S)}, \quad (2)$$

$$W_S = \frac{f_S R_\lambda}{f_S R_\lambda + (1 - f_S)}, \quad (3)$$

so

$$f_S = \left(\frac{R_\lambda}{W_S} - R_\lambda + 1 \right)^{-1}. \quad (4)$$

The Kurucz (1992) models were used to compute R_λ.

For double-lined systems, we modify the above formulae slightly. As before, we let R_λ represent the spot/nonspot surface flux ratio on the primary star (which is the more active star in all three stars we studied) and R'_λ represent the surface flux ratio between the photosphere of the secondary star and the nonspot photosphere of the primary. In this three-component model, we assume that the secondary is unspotted. The program then computes the best-fit weights of the nonspotted part of the primary star (W_Q), the spotted regions of the primary (W_S), and the secondary star ($W_{\rm sec}$); $W_Q + W_S + W_{\rm sec} = 1$. If we wish to compute the spot filling factor of the primary star, we must first subtract the contribution of the light from the secondary star. The fraction of the primary's light from the spots is

$$W'_S = \frac{W_S}{1 - W_{\rm sec}}. \quad (5)$$

The spot filling factor on the primary is then

$$f_S = \left(\frac{R_\lambda}{W'_S} - R_\lambda + 1 \right)^{-1}. \quad (6)$$

To model each spectrum, we used 3–5 different comparison stars for each component (nonspot photosphere, spots, and secondary when appropriate) of the active star system, spanning a range of $\approx$100–200 K both above and below the expected temperatures (from previous TiO studies) of each component. The f_S values from these fits were then averaged to derive the final f_S value for each active star observation. Intuitively, assuming a warmer spot should result in a larger f_S being computed to reproduce the observed OH line strength in the active star spectrum. This is the case for

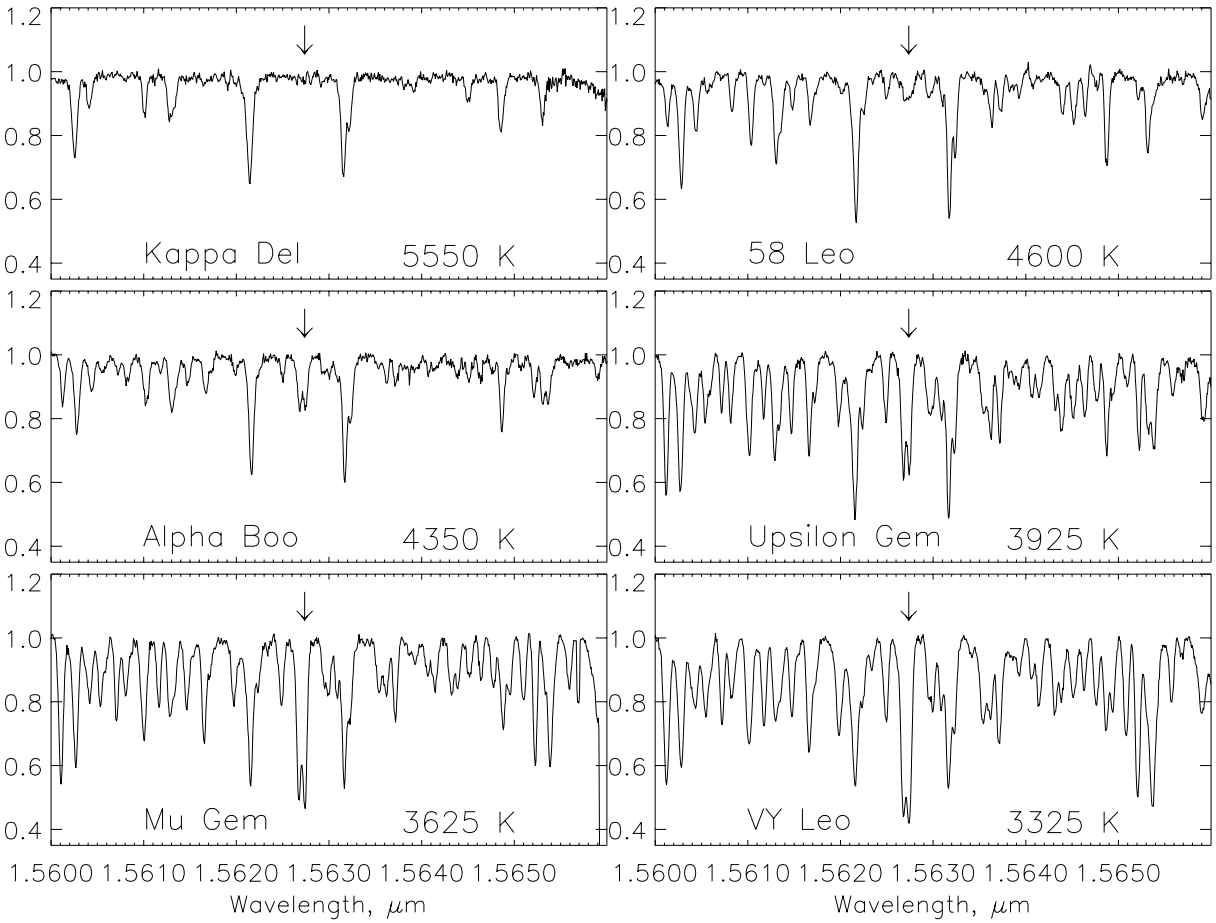

FIG. 1.—Phoenix spectra of a sample of the giant and subgiant comparison stars observed for this program. The position of the OH absorption lines is marked by an arrow; the feature is first visible around $T_{\rm eff} = 5000$ K and increases in strength with decreasing $T_{\rm eff}$.

$T_S \gtrsim 3500$ K, but below this T_S the relation levels off and f_S becomes largely independent of T_S—the lower R_λ for a cooler spot begins to compensate for the greater intrinsic OH line depth in the spot. This is the same behavior observed for the 8860 Å TiO band, but opposite that observed for the 7055 Å band (O'Neal, Neff, & Saar 1998, hereafter Paper III).

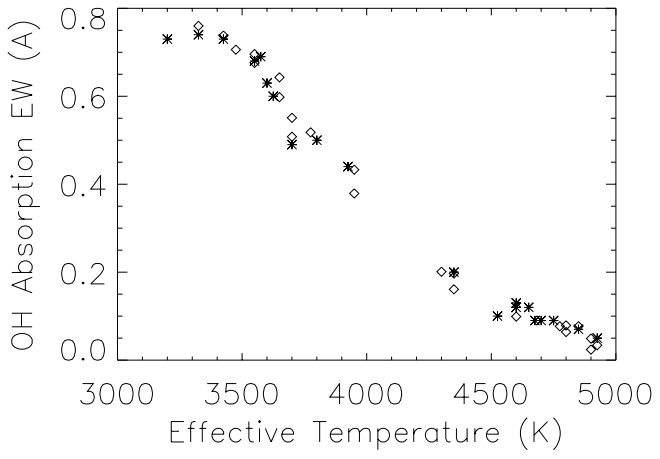

FIG. 2.—Relation between equivalent width of the OH 1.5627 μm feature and $T_{\rm eff}$ for giant and subgiant comparison stars. Equivalent width increases approximately linearly with decreasing $T_{\rm eff}$ from 5000 to 3000 K. Values for spectra observed with Phoenix are plotted as asterisks, while the NICMASS results (O'Neal & Neff 1997) are plotted as diamonds.

3.1. *II Peg = HD 224085*

II Peg is an extremely active single-lined, spectroscopic binary system with a spectral type K2–K3 IV–V and $v \sin i = 23$ km s^{-1}. It exhibits V-band variations of up to 0.6 mag (e.g., Byrne et al. 1995; Doyle et al. 1988). Using TiO bands, we have detected f_S as high as 56% (Paper II), finding $T_Q = 4800$ K and $T_S = 3500 \pm 100$ K. II Peg is highly spotted ($f_S \approx 0.25$) even at maximum brightness. Berdyugina et al. (1999) present Doppler images of the spot distribution on II Peg, finding large high-latitude ("polar") spots, and conclude that the total spot area on the star is approximately constant with time, merely distributing itself between different active longitudes over the star's activity cycle. Berdyugina et al. (1999) used a different ephemeris, but for our dates of observation it yields phases only 0.02 of a rotation behind those we have computed using the ephemeris in Vogt (1981).

We obtained six spectra of II Peg, spanning phases from 0.12 to 0.85, with a large gap due to poor weather on November 28 and 29. We fitted the spectra of II Peg using the nonspot comparison stars of $T_{\rm eff} = 4700$, 4750, and 4850 K, and we used spot comparison stars with $3425\ K \leq T_{\rm eff} \leq 3600$ K. Figure 5 shows the fit to the November 26 spectrum of II Peg, using comparison stars γ^2 Del ($T_{\rm eff} = 4700$ K) and TV Psc ($T_{\rm eff} = 3575$ K). The rms deviation of

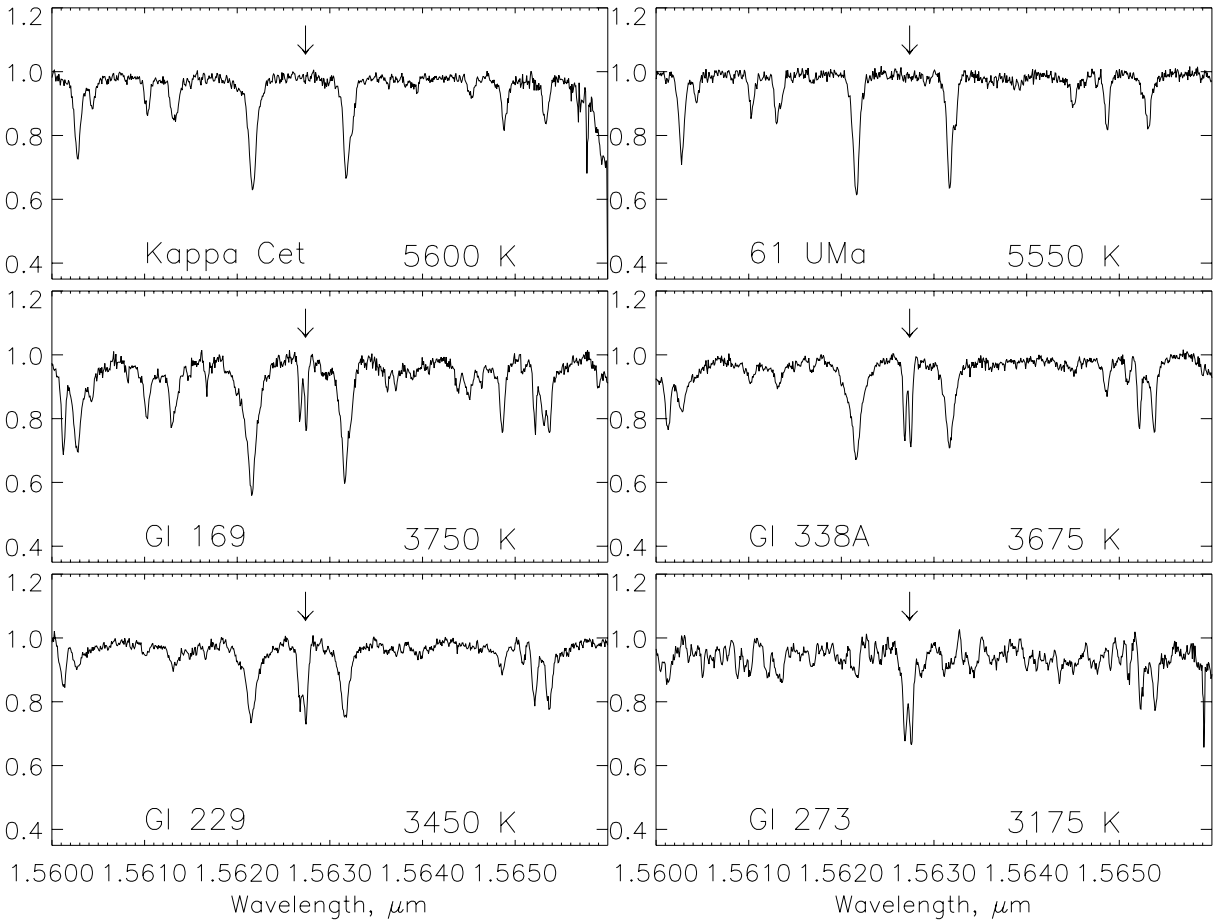

FIG. 3.—Phoenix spectra of a sample of the G, K, and M dwarf comparison stars observed for this program. The position of the OH absorption lines is marked by an arrow. The behavior of the OH feature with $T_{\rm eff}$ is similar for dwarfs and giants, but the feature is weaker in M dwarfs than in M giants of the same $T_{\rm eff}$.

this fit from the stellar spectrum is $\sigma = 0.016$; deviations between the model and the fit near the 1.5631 μm Fe I line are due to irreducible uncertainties in normalizing the various spectra.

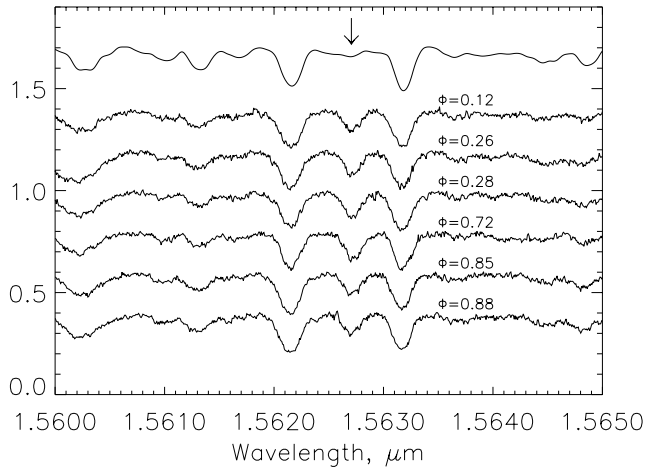

FIG. 4.—All six spectra of II Peg, vertically offset for clarity. The II Peg spectra are compared with the artificially rotationally broadened spectrum of an inactive star (γ^2 Del; *top*) of similar spectral type and $T_{\rm eff}$. Excess absorption caused by the OH molecule is marked with an arrow; the phase of observation is given for each spectrum.

During our observations f_S ranged from 0.35 at $\Phi = 0.88$ to 0.49 at $\Phi = 0.72$. We expect that the phase of maximum spot coverage should correspond to the star's photometric minimum at a given epoch. Photometry taken during 1998 October and December (Berdyugina et al. 1999) shows minimum light around $\Phi = 0.55$–0.60, consistent with our maximum f_S at $\Phi = 0.72$ (given that weather prevented our

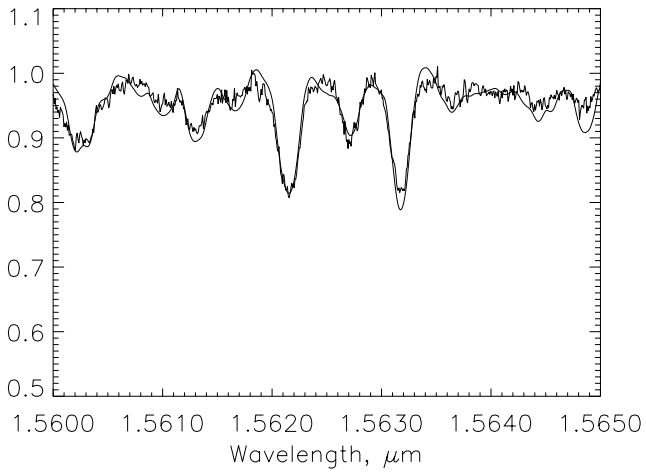

FIG. 5.—Fit to the II Peg spectrum of November 26 ($\Phi = 0.12$), using $T_Q = 4700$ K and $T_S = 3575$ K. The smooth line is the fit; $\sigma = 0.016$.

observations between phases 0.28 and 0.72). At this phase, one of the three high-latitude spots in their 1998 November Doppler image would have been closest to being centrally located on the star's disk.

The secondary star of the II Peg system has never been detected. If it is an M dwarf, IR observations would improve prospects for its detection, given the greater relative brightness of the cooler M star in the IR. Berdyugina et al. (1998) placed a limit of $M_v \geq 8.8$ on the II Peg secondary, the absolute magnitude of an early M dwarf. ON calculated that S/N $\approx$ 200 in our Phoenix spectra would be sufficient to detect an early M dwarf secondary. In that calculation, though, we neglected the fact that at most phases the secondary's lines would be Doppler shifted away from the corresponding lines from the primary. Assuming $R = 2.2\ R_\odot$ for the primary (Vogt 1981) and $R = 0.54\ R_\odot$ for a hypothetical M dwarf secondary star (Gray 1992), the 1.5623 and 1.5631 μm Fe I lines and the OH absorption from an early M dwarf secondary would appear at the same level as the noise for S/N $\approx$ 110. Given our actual S/N of 150–180, this would be just below a 2 σ detection.

Therefore, we first searched the II Peg spectra for small blips that might arise from strong lines of the secondary star. No consistent sets of three lines (two Fe I, one OH, with the proper λ spacing) were found in any of the spectra. For a more sensitive test, we co-added all six II Peg spectra *in the rest frame of the hypothetical secondary star*. We computed what the velocity separations between the two stars would be (at each observed phase), assuming an M dwarf mass of 0.5 $M_\odot$ and various primary masses from 0.8 to 2.5 $M_\odot$ (step size 0.05 $M_\odot$), shifted all the spectra to the rest frame of the secondary, and co-added them. When we did this for a primary mass of 2.05 $M_\odot$, we found in the co-added spectrum "lines" of a depth of 0.8%, at the proper positions of the Fe I and OH lines. It is intriguing to speculate that these might be due to an M dwarf secondary, but they are still barely above the level of the noise, and no positive conclusion can be drawn. Finally, we computed a model II Peg spectrum for stellar radii of 2.2 and 0.54 $R_\odot$, $f_S = 0.45$, T_S and T_Q as in Table 1, and Gl 96 ($T_{\rm eff} = 3525$ K) as a model for the secondary. The model predicts that strong lines of the secondary would depress fluxes by 0.7% $\pm$ 0.2% compared with a model without a secondary. Berdyugina et al. (1998) favor a greater radius but lower $T_{\rm eff}$ for the II Peg primary, 3.4 $R_\odot$, and 4600 K. Using these values, the lines from the secondary would reduce fluxes by only 0.4% compared with the situation without a secondary. In summary, our upper limits for the brightness of the II Peg secondary at this wavelength are similar to those given by Berdyugina et al. (1998) and Berdyugina et al. (1999).

3.2. *V1762 Cyg = HR 7275 = HD 179094*

This RS CVn binary with a K1 III–IV primary was recently discovered to be an SB2 (Osten & Saar 1997). The secondary is probably G8 V, giving a flux ratio of $\sim$35:1 at 1.56 μm, small enough that it can be neglected in our fitting procedures. Previously (Paper II and Paper III) we used TiO bands to derive $T_Q = 4550$ K, $T_S = 3450 \pm 150$ K, and f_S ranging from 0.10 to 0.27. ON found f_S at and slightly exceeding the upper end of that range. The system has a 28.6 day period, so our observations did not cover a large fraction of a rotational cycle. We computed f_S values ranging from 0.13 to 0.20 for our three Phoenix observations of V1762 Cyg. Figure 6 shows a fit to the December 1 spectrum, using comparison stars of $T_{\rm eff} = 4600$ and 3425 K; $\sigma = 0.013$.

3.3. *λ And = HR 8961 = HD 222107*

The second-brightest RS CVn system (after Capella), λ And is a nonsynchronous rotator, with $P_{\rm rot} = 54.05$ days but $P_{\rm orb} = 20.5$ days. The visible component of this single-lined binary is a G8 III–IV star with $T_{\rm eff} = 4750 \pm 30$ K, $v \sin i = 6.5$ km s^{-1}, and $\log g = 2.5$ (Donati, Henry, & Hall 1995). In Paper III we derive $T_S = 3650 \pm 150$ K and f_S between 0.14 and 0.23. ON found f_S values between 0.22 and 0.26.

In Table 2 we list the f_S values found in this study for λ And. Figure 6 shows the fit to the November 26 spectrum; $\sigma = 0.020$.

3.4. *σ Gem = HD 62044*

σ Gem, like the rest of the stars described below, was not observed by ON. It is an SB1 with a K1 III spectral type, a 19.4 day period, and $v \sin i = 25$ km s^{-1}. In Paper II and Paper III, we found (using TiO bands and contemporaneous photometry) $T_Q = 4500$ K, $T_S = 3850$ K, and f_S ranging from 0 to 0.33 over 10 epochs of observations. To fit the Phoenix observations, we used nonspot comparison stars with $T_{\rm eff} = 4525$ and 4600 K and the three-spot comparison stars with $T_{\rm eff} \geq 3700$ K.

Computed f_S values range from $\sim$0 to 0.15, with the highest value observed on November 27. In Figure 6 we present a fit to the November 27 spectrum, using comparison stars with $T_{\rm eff} = 4525$ and 3800 K and $\sigma = 0.014$.

3.5. *LQ Hya = HD 82558*

LQ Hya is a single K2 V star, which might only recently have arrived on the main sequence (Fekel et al. 1986). Rice & Strassmeier (1998) present Doppler images of this star, and they find spots concentrated near the equatorial regions instead of at high latitudes. Saar (2000) analyzed

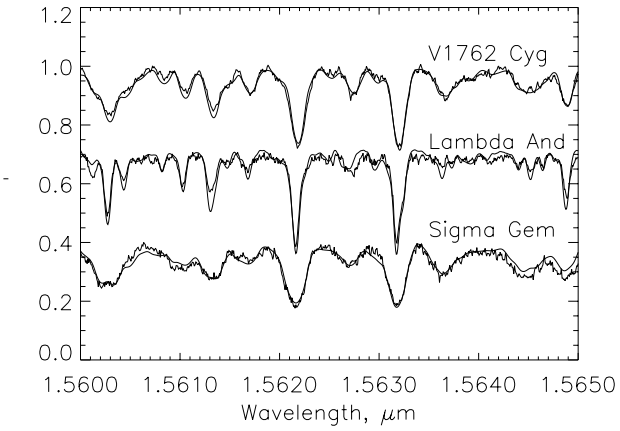

FIG. 6.—*Top*, spectrum of V1762 Cyg obtained on December 1, and the best fit (*smooth line*) to it, using nonspot and spot comparison stars of 4600 and 3425 K, respectively; $\sigma = 0.013$; *middle*, spectrum of λ And obtained on November 26 and the best fit ($\sigma = 0.020$) using nonspot and spot comparison stars of 4850 and 3625 K, respectively; *bottom*, spectrum of σ Gem obtained on November 27 and the best fit ($\sigma = 0.014$) using nonspot and spot comparison stars of 4525 and 3800 K, respectively.

TiO-band observations of LQ Hya and found $T_Q = 5175$ K, $T_S = 3650$ K, and f_S values of 0.50 ± 0.12; f_S was uncertain because of the intrinsically weak TiO bands in the star's spectrum.

Our grids of dwarf comparison stars consist of only three G/K stars and six M stars. Since none of these stars are near the T_Q of LQ Hya, we fixed the $T_Q = 5175$ K and used the available G/K dwarf spectra. Changing the nonspot model turned out to make little difference, $\Delta f_S < 0.02$. The best fits were obtained using Gl 1338A9, with $T_{\rm eff} = 3675$ K, as a model for the spotted regions of LQ Hya. In Figure 7 we illustrate a fit to the November 30 spectrum of LQ Hya. For this spectrum $f_S = 0.45$; $\sigma = 0.019$.

3.6. *Gl 171.2A = V833 Tau = HD 283750*

We obtained one spectrum of this active K4 V star. Saar (2000) found $T_Q = 4500$ K, $T_S = 3175$ K, and $f_S = 0.51 \pm 0.01$. We obtained no spectra of inactive dwarf stars with T_Q similar to Gl 171.2A, so we used a spectrum of κ Cet and fixed T_Q to 4500 K in our fits. From spectra shown in ON, the OH absorption has not appeared in dwarfs at a temperature of 4850 K. If this is still true at 4500 K, then our fits will not be substantially affected by using a comparison star this much warmer than T_Q.

The two coolest M dwarf comparison stars, Gl 15A and Gl 273, have weak Fe I lines (a spectrum of Gl 273 is shown in Fig. 3), but this seems to be largely a $T_{\rm eff}$ effect, since both stars have metallicities near solar (within ± 0.02 dex; Eggen 1996). Thus, despite the weak Fe I lines, Gl 273 ($T_{\rm eff} = 3175$ K), specifically, can be used as the proxy for the spotted regions of Gl 171.2A. We fitted only the region immediately around the OH absorption and obtained $f_S = 0.45$ and the fit shown in Figure 7 ($\sigma = 0.017$). The poor fit to the Fe I lines results from their weakness in the spot comparison spectrum. In addition, for this star as well as for OU Gem, the lack of a proper T_Q comparison diminishes the quality of the fits to the atomic lines.

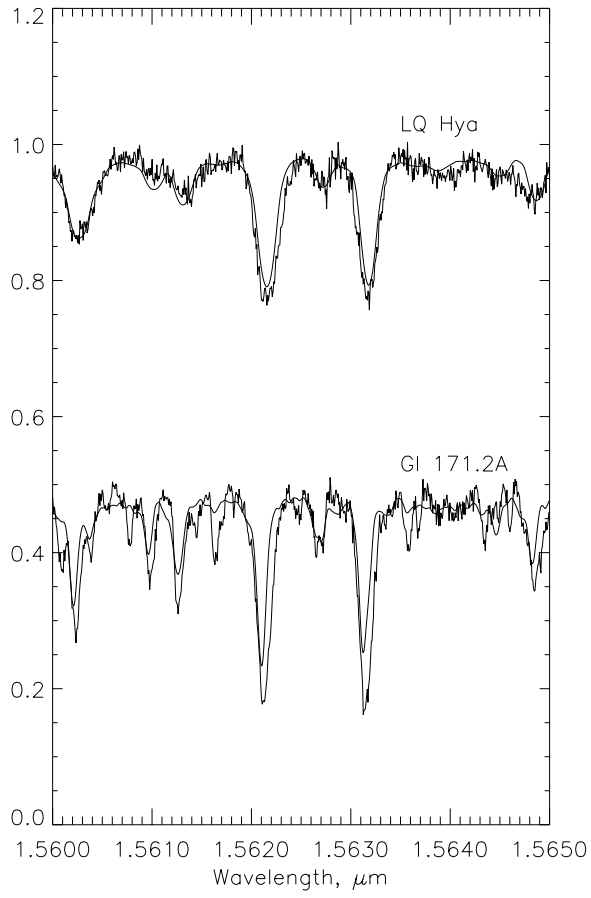

FIG. 7.—*Top*, November 30 spectrum of LQ Hya and a fit to it, assuming $T_Q = 5175$ K and $T_S = 3675$ K; $\sigma = 0.019$; *bottom*, our spectrum of Gl 171.2A (obtained November27) and the fit to it, assuming $T_Q = 4500$ K and $T_S = 3175$ K; $\sigma = 0.017$.

3.7. *UX Ari = HD 21242*

UX Ari is an SB2 (G5 V + K0 IV) in which the cooler star is more magnetically active (Montes et al. 1996 and references therein). It is one of the few RS CVn systems (others include II Peg and HR 1099) that always shows Hα in emission above the continuum.

This is the first time we have attempted to use our spectral synthesis technique to measure starspot coverage on the active component of a double-lined binary. The G5 V and K0 IV components of UX Ari have $v \sin i$ values of 6 and 37 km s^{-1}, respectively. We used both η Cep and HR 7794 to model the nonspotted photosphere of the primary star (the brighter K0 IV component of the system). These are both slightly cooler than the 5000 K derived by Elias et al. (1995) but are consistent with the primary's spectral type. BY Boo was our proxy for the spots on the primary, and we used both κ Cet and 61 UMa as models for the secondary (G5 V) star. We computed the radial velocity difference between the stars expected at the phase of each observation and used that as an initial guess (input into STARMOD) for the radial velocity of the secondary star. At $\Phi = 0$, the primary star is in front as seen from Earth.

Elias et al. (1995) give radii of 3.60 and 1.71 $R_\odot$ for the primary and secondary stars, respectively. Using these radii and the R_λ appropriate to the stars' $T_{\rm eff}$ values (Table 3), we calculate $W_{\rm sec} = 0.21$. Using a more typical radius for a G5 V star, 0.96 $R_\odot$ (Gray 1992), gives $W_{\rm sec} = 0.08$. Both these values assume that the primary has negligible spot coverage; if it had a substantial spot coverage, $W_{\rm sec}$ would increase accordingly. If, on the other hand, the secondary had $f_S = 0.5$, $W_{\rm sec}$ (in this case, the total light from the nonspot and spot regions of the secondary) would decrease to 0.05 for a 0.96 $R_\odot$ secondary. Even this large spot coverage on the secondary would produce a small effect in the overall spectrum; it would reduce the continuum light level by 2.6% at the position of the secondary's OH line. Given that in many phases the secondary's OH is blended with an Fe I line of the primary, this would be difficult to detect. In phases where the two stars have similar v_r, it would only mimic $f_S = 0.05$ on the primary, at the limit of our ability to detect.

In our fits, we found that values of $W_{\rm sec}$ between 0.11 and 0.14 provided the best fits to the strengths of the secondary's lines in the UX Ari spectra. Combining these values and our derived f_S, we find that the most likely radius for the UX Ari secondary (assumed unspotted) is 1.25 ± 0.1 $R_\odot$.

Fitting the spectra of UX Ari using the stated parameters yielded a range of spot filling factors, from 0.11 (November 27) to 0.48 (December 2). It may be that there was a large starspot in the Earth-facing hemisphere at the $\Phi = 0.95$ of the December 1 observation ($f_S = 0.42$; the f_S value for December 2 should be considered less certain than the

others because no Rigel spectrum was available to complete the normalization process). This would place it on the part of the star's surface facing almost directly away from the secondary star. Figure 8 shows the fit to the November 26 spectrum. The narrower dip inside the broad OH absorption is the 1.5631 μm Fe I line of the secondary star. This fit gives $f_S = 0.26$ and $W_{sec} = 0.15$; $\sigma = 0.010$.

3.8. *HR 1099 = V711 Tau*

This extensively studied SB2 RS CVn system consists of a K1 IV primary star and a G5 IV secondary star in a 2.8 day orbit ($\Phi = 0$ indicates that the primary is in front). The K1 star is the faster rotator (40 km s^{-1} compared with 13 km s^{-1} for the secondary; Vogt et al. 1999), and most studies of the HR 1099 system have placed the starspots primarily or exclusively on the primary (e.g., Henry et al. 1995; Vogt et al. 1999). Vogt et al. (1999) found a persistent (from 1981 to 1992) polar spot of variable size on the primary, combined with transient low-latitude dark spots; a major dark spot on this star can significantly evolve on a timescale of a few months.

Hatzes et al. (1996) give $T_Q = 4700$ K and $T_S = 3500$ K for the primary star; Vogt et al. (1999) give $T_Q = 4750$ K and threshold their Doppler images to $\Delta T = T_Q - T_S = 1200$ K. For our fits, we used γ^2 Del as the model for the primary's photosphere, BY Boo for the starspots, and κ Del for the secondary star. Using $R = 3.9$ and 1.3 $R_\odot$ for the primary and secondary stars (Fekel 1983), $W_{sec} = 0.12$ for an unspotted primary.

We found f_S values ranging from 0.0 to 0.40. The fit to the HR 1099 spectrum of November 26 ($\Phi = 0.08$ is shown in Figure 8; $\sigma = 0.013$. At this phase, orbital motion gives a net 5.7 Å blueshift for the secondary star's lines, blending its 1.5631 μm Fe I line with the primary's OH line.

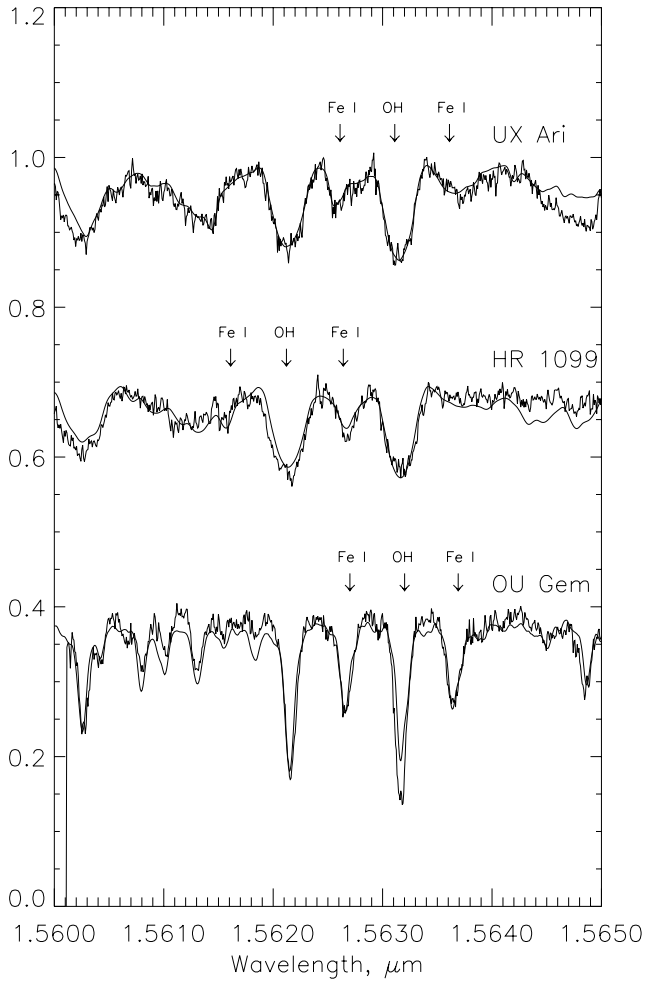

FIG. 8.—*Top*: Spectrum of November 26 of the SB2 RS CVn system UX Ari, with a fit ($\sigma = 0.010$) using HR 7794 as a proxy for the nonspotted regions of the primary star, BY Boo as the spot proxy, and κ Cet as the proxy for the secondary star. This fit gives $f_S = 0.26$ for the primary star and $W_{sec} = 0.15$. *Middle*: November 26 spectrum of HR 1099, with a fit ($\sigma = 0.013$) using γ^2 Del as the proxy for the primary star's nonspotted regions, BY Boo for the primary's starspots, and κ Del for the secondary star. This fit gives $f_S = 0.07$ for the primary star. *Bottom*: November 30 spectrum of OU Gem, with a fit ($\sigma = 0.023$) using κ Cet as a proxy for the nonspotted photospheres of both components of the system and Gl 96 as a proxy for starspots on the primary star; $f_S = 0.22$ and $\sigma = 0.021$. In each of these SB2 spectra, arrows indicate the positions of the OH line and the 1.5623 and 1.5631 μm Fe I lines of the secondary star.

3.9. *OU Gem = HD 45088*

This system consists of two dwarf stars (K3 V and K5 V) in a 7 day orbit with an eccentricity $e = 0.15$. OU Gem has a much lower (more nearly equal) brightness ratio between the two components than do the other SB2 systems we study. $\Phi = 0$ denotes the primary star being farthest from the observer. The hotter star is more active than the cooler star, although both components have the Ca II IRT and Ca II H and K lines in emission (Montes et al. 2000).

In our November 26 and 27 OU Gem spectra, the 1.5631 μm Fe I line from the secondary star is blended with the primary's OH line. In the November 30 spectrum, the relative v_r have reversed so that the 1.5623 μm Fe I line of the secondary is blended with the primary's OH. The final spectrum (December 1) was taken close to the time of conjunction, yielding $\Delta v_r \sim 0$; it shows only a weak absorption in the position of the OH lines.

We used the κ Cet spectrum as a proxy for both stars of the system and fixed T_{eff} at 4925 and 4550 K for the primary and secondary, respectively. Lacking information on a possible T_S, we used Gl 96 ($T_{eff} = 3525$ K) as a model for starspots in the system; we ran trials with starspots on both components. Assuming no starspot coverage on either component and using the T_{eff} values and radii for K3 V and K5 V stars given in Gray (1992), $W_{sec} = 0.39$.

For the December 1 spectrum, the total f_S for the two stars was at most 0.04. The other three spectra were fitted best by invoking starspots on the primary star, with f_S ranging from 0.20 to 0.35. The fit to the spectrum of November 30 is shown in Figure 8; $\sigma = 0.021$. The blended line consisting of the primary's OH and one of the Fe I lines from the secondary is fitted quite well; good fits also are obtained in this spectrum and others to the Fe I lines from the primary that are *not* superposed where the OH from the secondary would be.

On the other hand, the 1.5623 μm Fe I line (for November 27) and the 1.5631 μm Fe I line (for November 30)—both presumably blended with OH absorption from the secondary star—are not fitted well. The blend primary Fe I + secondary OH in the model should be *deeper* in both cases to fit the observed spectra. This raises the possibility that there is some starspot coverage on the secondary star as well. However, to obtain better fits to the primary Fe I + secondary OH blends, it was necessary to invoke huge spot filling factors, greater than 0.6, on the

secondary star. We consider this unlikely, given that a low f_S is detected at the one phase we observed at which this blend does not happen; also, it is implausible that such a huge spot area seen at $\Phi = 0.89$ (November 27) would not be visible one night earlier ($\Phi = 0.74$), when the fit to the blend primary Fe I + secondary OH needs no adjustment. It is more likely that the Fe I lines of κ Cet are imperfect models for the Fe I lines of either or both components of OU Gem.

4. DISCUSSION

Three of the stars observed in this program were also observed by ON: V1762 Cyg, λ And, and II Peg. In the case of V1762 Cyg, the f_S values observed in this study ($0.13 \leq f_S \leq 0.20$) were somewhat less than those found by ON ($0.27 \leq f_S \leq 0.32$). For λ And and II Peg, the f_S values measured in the two studies fell within the same range. This suggests that there is no systematic effect that appears because of the higher resolution of the Phoenix spectrograph ($R \approx 60{,}000$) as compared with that of NICMASS ($R \approx 26{,}000$). $R = \lambda/\Delta\lambda = 26{,}000$ corresponds to a $v \sin i \approx 6$ km s^{-1} at this wavelength, and six of the nine active systems studied here have $v \sin i$ (of the active component) notably greater than this. This paper uses a much more sensitive detector than ON (see § 1); whereas ON obtained poor S/N spectra of II Peg, Phoenix would be capable of obtaining reasonably good S/N on stars at least 2 mag (H band) fainter.

High-resolution infrared spectroscopy is still a rather young observational technique, spurred by the rapid growth of infrared detector technology. Only a few high-resolution IR spectrographs exist. Better phase coverage on our target stars would be desirable, but that may have to wait until sensitive IR spectrographs are more widely available.

Unlike our TiO band technique detailed in Papers I, II, and III, the OH technique uses only one spectral feature and thus cannot place independent constraints on f_S and T_S. One must assume a T_S or derive it by using some other method before f_S can be calculated. But once T_S is known, the OH technique, like the TiO band method, determines an f_S that represents an *absolute* measure of the starspot coverage, regardless of the spatial distribution of the spots. Traditional photometric light-curve modeling can measure only an asymmetric spot distribution, or differences from an *assumed* "immaculate" light level; a longitudinally symmetric spot distribution produces no variation in the star's brightness. Doppler imaging (DI) also often misses a symmetric spot component.

In an important sense, our OH line technique is complementary to Doppler imaging. The OH method works best at lower $v \sin i$ values where DI is ineffective. Conversely, DI is superior at high $v \sin i$, since for $v \sin i \gtrsim 50$ km s^{-1}, the OH lines begin to blend with the nearby strong Fe I features, rendering their measurement more difficult. There is a substantial overlap in the applicability of the two techniques; II Peg ($v \sin i = 23$ km s^{-1}), for example, is easily studied by both methods (e.g., Berdyugina et al. 1999). In a future study, we plan to apply DI techniques to some of the data presented here and in ON to derive maps of starspot coverage based on IR spectra. The OH spectra will give us the ability to determine a true f_S value for each spectrum, constraining the small-size-scale symmetric spot component that DI often misses. DI can provide the actual maps of starspot coverage that are not possible to derive from OH measurements of f_S alone.

There are several advantages gained from observing starspots in the OH absorption lines rather than in TiO bands. First, R_λ is much greater in this spectral region than in the visible, so starspots have a greater effect in the overall spectrum. In this study, we have measured f_S values as low as 0.06, a substantial improvement on the lower limit to the sensitivity of the TiO band technique ($\sim$0.10–0.12). Also, unlike with the TiO method, starspots warmer than 4000 K will be detectable in OH. Spots in this temperature range have been found for some active stars, including HD 32918 (Piskunov, Tuominen, & Vilhu 1990). We estimate that in an active star with $T_Q = 4800$ K, $f_S = 0.32$, and $T_S = 4400$ K, the OH lines used here would have an equivalent width of 0.1 Å, compared with 0.06 Å for an unspotted star of the same $T_{\rm eff}$. Finally, analysis of the OH lines is easier in SB2 systems than the complex extended TiO bands.

The uncertainties given in Table 2 are statistical errors. They were computed by, first, fitting an active star spectrum with one nonspot comparison star and several (usually 3–5) spot comparison stars of $T_{\rm eff}$ near that of the assumed T_S of the active star. Taking the f_S values for these fits gave us an average f_S with an uncertainty equal to one-half the total range of f_S values for those fits. We then used 1–3 other *nonspot* comparison stars to compute the fits and computed an average f_S and uncertainty for the fits using each nonspot comparison star. Averaging these f_S values and their uncertainties gave us the entries in Table 2.

There are two primary sources of systematic error in this technique. First is the basic concern as to how well the spectrum of an inactive star of temperature $T_{\rm eff}$ can stand as a proxy for a starspot with $T_S = T_{\rm eff}$. This error is difficult to quantify without detailed starspot atmosphere models. The second main source of systematic error (for active subgiants) is uncertainty about whether molecular features in giants are good proxies for starspots on subgiants (only σ Gem is unambiguously assigned to luminosity class III). In Paper I we showed that the TiO bands are as much as 5 times deeper in giants than in dwarfs of the same $T_{\rm eff}$, and the same strengthening of the molecular features with decreased gravity can be seen in OH. In Paper II we discuss the possible effects of log g on the spectra of starspots and estimate that the error introduced by using giant spot proxies for subgiant active stars is an underestimate of perhaps 0.1 in f_S.

Results of TiO band measurements have already yielded important insights into the thermal and magnetic properties of stellar spots (e.g., Saar et al. 2000). Simultaneous observations of active stars in TiO bands and in the OH features would be useful. The TiO bands can independently measure T_S, whereas the OH lines provide a more sensitive measure of f_S, especially for warmer T_S. Possible variations in T_S among spots can also be studied in more detail (e.g., O'Neal, Saar, & Neff 1998). Contemporaneous photometry would also be valuable in constraining T_S and f_S (e.g., Paper III). Combined with simultaneous Doppler imaging, OH and TiO data should lead to a much more nearly complete understanding of spatial and physical properties of starspots. There now exist molecular line data of sufficient quality (e.g., Valenti, Piskunov, & Johns-Krull 1998) that we will soon be able to model directly the molecular features in the nonspot and spot stellar atmospheres. Comparing these results with those using our nonspot and spot

proxies will provide valuable information on the question of how well proxies model spot atmospheres and on the reliability of both our technique and the molecular line lists.

5. SUMMARY

We have analyzed spectra of nine late-type magnetically active stars—six RS CVn systems and three active dwarf stars—in the H-band region near 1.563 μm containing the 6397 cm^{-1} (1.563 μm 3–1 P2e and P2f [$J = 5.5$]) transitions of the OH molecule. In spectra of inactive stars, the equivalent width of these OH lines increases as T_{eff} decreases from 5000 to 3000 K. We clearly see excess OH absorption in the active star spectra compared with rotationally broadened spectra of inactive comparison stars of the same T_{eff}. For six of our active stars, this is the first measurement of starspot parameters using OH lines. Also for the first time, we have been able to use molecular spectral features to measure the starspot filling factors of active components of double-lined spectroscopic binaries. This technique greatly increases (by $\sim$1000 K) the range of starspot temperatures that can be studied via molecular absorption features.

We thank Ken Hinkle and Jeff Valenti for their assistance with using the Phoenix spectrograph. This work was supported by *Hubble Space Telescope* grant GO-6676 (S. H. S.). J. K. M. acknowledges the financial support of Washington and Jefferson College. This research made use of the SIMBAD database, operated at CDS, Strasbourg, France.

REFERENCES

Barden, S. C. 1985, ApJ, 295, 162
Berdyugina, S. V., Berdyugin, A. V., Ilyin, I., & Tuominen, I. 1999, A&A, 350, 626
Berdyugina, S. V., Jankov, S., Ilyin, I., Tuominen, I., & Fekel, F. C. 1998, A&A, 334, 863
Bopp, B. W., & Dempsey, R. C. 1989, PASP, 101, 516
Bopp, B. W., Hall, D. S., Henry, G. W., Noah, P., & Klimke, A. 1981, PASP, 93, 504
Boyd, R. W., et al. 1983, Ap&SS, 90, 197
Byrne, P. B., et al. 1995, A&A, 299, 115
Claret, A., Diaz-Cordoves, J., & Giminez, A. 1995, A&AS, 114, 247
Donati, J.-F., Henry, G. W., & Hall, D. S. 1995, A&A, 293, 107
Doyle, J. G., Butler, C. J., Morrison, L. V., & Gibbs, P. 1988, A&A, 192, 275
Eggen, O. J. 1996, AJ, 111, 466
Elias, N. M., II, Quirrenbach, A., Witzel, A., Naundorf, C. E., Wegner, R., Guinan, E. F., & McCook, G. P. 1995, ApJ, 439, 983
Fekel, F. C. 1983, ApJ, 268, 274
Fekel, F. C., Bopp, B. W., Africano, J. L., Goodrich, B. D., Palmer, L. H., Quigley, R., & Simon, T. 1986, AJ, 92, 1150
Gray, D. F. 1988, Lectures on Spectral Line Analysis: F, G, and K Stars (Arva, Ontario: The Publisher)
———. 1992, The Observation and Analysis of Stellar Photospheres (2d ed.; Cambridge: Cambridge Univ. Press)
Grevesse, N., Sauval, A. J., & van Dishoeck, E. F. 1984, A&A, 141, 10
Hatzes, A. P., Vogt, S. S., Ramseyer, T. F., & Misch, A. 1996, ApJ, 469, 808
Henry, G. W., Eaton, J. A., Hamer, J., & Hall, D. S. 1995, ApJS, 97, 513
Hinkle, K. H., Cuberly, R., Gaughan, N., Heynssens, J., Joyce, R., Ridgway, S., Schmitt, P., & Simmons, J. E. 1998, Proc. SPIE, 3354, 810
Hinkle, K., Wallace, L., & Livingston, W. 1995, Infrared Atlas of the Arcturus Spectrum, 0.9–5.3 Microns (San Francisco: ASP)
Hoffleit, D., & Jaschek, C. 1982, The Bright Star Catalogue (4th ed.; New Haven: Yale Univ. Obs.)
Jetsu, L. 1993, A&A, 276, 345
Kurucz, R. L. 1992, Rev. Mexicana Astron. Astrofis., 23, 45
Montes, D., Fernández-Figueroa, M. J., de Castro, E., Cornide, M., Latorre, A., & Sanz-Forcada, J. 2000, A&AS, 146, 103
Montes, D., Sanz-Forcada, J., Fernández-Figueroa, M. J., & Lorente, R. 1996, A&A, 310, L29
Neff, J. E., O'Neal, D., & Saar, S. H. 1995, ApJ, 452, 879 (Paper I)
Oláh, K., & Pettersen, B. R. 1991, A&A, 242, 443
O'Neal, D., & Neff, J. E. 1997, AJ, 113, 1129 (ON)
O'Neal, D., Neff, J. E., & Saar, S. H. 1998, ApJ, 507, 919 (Paper III)
O'Neal, D., Saar, S. H., & Neff, J. E. 1996, ApJ, 463, 766 (Paper II)
———. 1998, ApJ, 501, L73
Osten, R. A., & Saar, S. H. 1997, MNRAS, 295, 257
Piskunov, N. E., Tuominen, I., & Vilhu, O. 1990, A&A, 230, 363
Rice, J. B., & Strassmeier, K. G. 1998, A&A, 336, 972
Saar, S. H., Peterchev, A., O'Neal, D., & Neff, J. E. 2000, in ASP Conf. Ser. 223-CD 1057, Cool Stars, Stellar Systems, and the Sun: Eleventh Cambridge Workshop, ed. R. J. García López, R. Rebolo, & M. R. Zapatero Osorio (San Francisco: ASP)
Stauffer, J. R., & Hartmann, L. W. 1986, ApJS, 61, 531
Strassmeier, K. G., Hall, D. S., & Henry, G. W. 1994, A&A, 282, 535
Valenti, J. A., Piskunov, N. E., & Johns-Krull, C. M. 1998, ApJ, 498, 851
Vogt, S. S. 1981, ApJ, 247, 975
Vogt, S. S., Hatzes, A. P., Misch, A. A., & Kürster, M. 1999, ApJS, 121, 547
Wallace, L., & Livingston, W. 1991, An Atlas of the Solar Spectrum in the Infrared from 1850 to 9000 cm^{-1} (1.1 to 5.4 Microns) (NSO Tech. Rep. 91-001) (Tucson: NSO)
———. 1992, An Atlas of a Dark Sunspot Umbral Spectrum from 1970 to 8640 cm^{-1} (1.16 to 5.1 Microns) (NSO Tech. Rep. 92-001) (Tucson: NSO)
Wamstecker, W. 1981, A&A, 97, 329
Welty, A. D., & Wade, R. A. 1995, AJ, 109, 326